Visible Light Communications with OLEDs for D2D Communications Considering User's Movement and Receiver Orientations

ZAHRA NAZARI CHALESHTORI,[1] STANISLAV ZVANOVEC,[1,*] ZABIH GHASSEMLOOY,[2] MOHAMMAD-ALI KHALIGHI,[3]

[1]*Department of Electromagnetic Field, Faculty of Electrical Engineering, Czech Technical University in Prague, Prague, Czech Republic.*
[2]*Optical Communications Research Group, Faculty of Engineering and Environment, Northumbria University, Newcastle-upon-Tyne, UK.*
[3]*Aix-Marseille University, CNRS, Centrale Marseille, Institut Fresnel, Marseille, France.*
**xzvanove@fel.cvut.cz*

Abstract: With the increasing use of organic light emitting diodes (OLED) in lights, smart phones, wearables smartwatches and computers, visible light-based device-to-device (D2D) communications become more and more relevant. This paper proposes D2D communications using the smart phone's display pixels and their built-in cameras. We investigate the impact of receiver orientation and user's mobility on the link performance. We derive a Gaussian model for the probability density function of the delay spread and optical path loss (OPL), and show that the channel delay spread decreases for a typical furnished room compared with an empty room, whereas the former has an increased OPL. In addition, we show that for the case of a furnished room and considering user mobility, the peak OPL values are about 64 and 62 dB, with and without considering the receiver's random orientation, respectively.

1. Introduction

In visible light communications (VLCs), inorganic and organic light emitting diodes (LEDs) and laser diodes (LDs) could be used as the light sources to provide illumination and data communications simultaneously [1, 2]. Note, inorganic LD-based lights should be diffused to meet the eye-safety. Organic LEDs (OLEDs), which use polymers or small organic molecules as their optically active element, offer unique features such as wide emission spectrum, high output, transparent display, high colour purity, low power consumption, compact, flexible substrates, and higher response rates (by 200 times), compared with the liquid crystal display (LCD) devices. These make OLEDs ideal in a number of applications including panels, displays of wearable smartwatches, computers, smartphones, and televisions [3, 4]. In smart devices, OLED displays together with the built in cameras could facilitate device-to-device (D2D) communications as part of the Internet of everything.

In VLC systems, in line with wireless communications, the channel impulse response (CIR) is mostly characterized in terms of the root-mean-square (RMS) delay spread τ_{RMS} and the average optical path loss (OPL). The former determines how susceptible the channel is to inter-symbol interference (ISI), which leads to reduced data rate R_b (if no post transmission channel equalization is to be done) [1, 5]. In [6], the CIR of an empty room of dimension 5×5×3 m^3 was evaluated using Monte Carlo (MC) ray tracing at the visible wavelength range. However, reflectance for surface materials was assumed to be wavelength-independent. The wavelength-dependent reflectance from surfaces was characterized for the first time in [7], where it was shown that the total diffuse power and τ_{RMS} for the VLC system were lower compared with the infrared transmission system. However, the effect of reflectance from furniture/objects in typical indoor environments on the CIR was not investigated. In recent years we have seen a growing use of software-based simulation packages in VLC. For instance, in [8] a three-dimensional computer-aided design (CAD) model was used for estimating the CIR of indoor VLC links based on Monte Carlo simulation approach. Opticstudio software from Zemax [9] has also been utilized for channel modelling in [10] that investigated the effect of reflectance from furniture in indoor environments on the CIR ; these results were later used in the IEEE 802.15.7r1 Task Group [11]. More recently, a new expression was developed for the CIR of an indoor VLC by considering the positions, sizes, and shapes of obstacles [12]. In [12], the LED illumination area was divided into independent solid angles and beam steering was used for the ray transmission in every solid angle. The impact of using flexible OLED in VLC was studied and compared with the case of Lambertian sources, where lower τ_{RMS} and the average OPL values of ~9% and 3 dB, were reported [13]. In [14], the use of OLED-based VLC (OVLC) for some indoor environments (i.e., office, shopping mall, corridor and semi-open corridor) were investigated, a data rate of 4 Mb/s was reported for the office environment using both curved and flat OLEDs at the transmitter's (Tx) half-angle within the range of ±90° and ±53°, respectively. Additionally, the authors showed that, for a semi-open corridor, the OPL values for the empty corridor and for a 10 m link span were lower by 6 dB compared with the furnished corridor. In [15], an indoor multi-user VLC system based on the angle diversity Tx was proposed that could achieve a higher data rate. Therein, the non-sequential ray-tracing method was used for estimating the CIR, where the authors also introduced an algorithm to eliminate the effect of interference from the different LOS links. Next in [16], the ray-tracing model was used to estimate the channel characteristics for an indoor MIMO VLC system using arrays of LEDs and PDs as well as two aspheric convex and concave lenses. Signal combination at the Tx and successive interference cancellation at the receiver (Rx) were adopted to improve the channel capacity. In [17], the good match between the simulation (using Opticstudio) and experimental results of channel characteristics was demonstrated for a MIMO VLC system in a furnished conference room.

Organic-based light sources are being widely used in a number of applications including shopping malls, offices, airports, etc., because of their flexibility, smooth lighting, etc. The eye-safety studies of OLED compared with non-organic LED light have revealed that retinal pigment epithelium (RPE) and photoreceptors can be damaged by the latter [18]. Typically, the so-called white phosphor LEDs (WPLEDs) use a blue LED, which has a Cerium-doped Yttrium Aluminum Garnet (Ce:YAG) yellowish phosphor encompassing the photoactive area. The blue wavelength is in fact the main reason of the functional damage. On the other hand, OLEDs are made by combining their emitting colors (i.e., wavelengths), which are more eye-safe than the non-organic LEDs, as the blue light intensity is not as high as that for WPLEDs for the same overall luminance level [18, 19]. Indeed, thanks to their higher brightness levels, wider color ranges, transparency, and improved durability, there has recently been a growing use of the organic technology in the applications such as display or in mobile and smart devices screens. Given these wide spread use of OLEDs, it is quite relevant to consider them as optical Txs for use in the Internet-of-things applications, in particular for short range and low data rate scenarios. In fact, there has been a limited amount of research reported on the utilization of OLED-based VLC (OVLC) in D2D communication systems, which has been the motivation behind this work.

In this paper, an OVLC scheme for D2D communications is considered for a typical office environment with furniture. We consider two static users that face each other and investigate the impact of the Rx's random orientations and the user's movement on the RMS delay spread and the OPL.

The rest of the paper is organized as follows. In section 2, the simulation environment is described, which includes the adopted scenarios and system modelling of Rx orientation and mobility. In section 3, the results are discussed. Finally, conclusions are given in section 4.

2. Simulation Environment

Here, we consider a three-dimensional indoor environment with a specific geometry including furniture, as depicted in Fig. 1. Also defined are the types and reflection coefficients of materials with respect to the wavelength and specifications of the both Tx and Rx. For the considered scenario, we have used the non-sequential ray tracing method to determine the detected optical power and the path lengths between the Tx and the Rx. Note, the CIR is expressed as [20]:

$$h(t) = \sum_{i=1}^{N} P_i \delta(t - \tau_i), \tag{1}$$

where P_i and τ_i are the power and the propagation time of the ith optical ray, respectively. δ is Dirac delta function, and N is the number of rays received at the Rx.

2.1 Scenarios

As shown in Fig. 1, two users are communicating with each other, where the display and the camera of the mobile phones are considered as the Tx and the Rx, respectively. Next, we consider three scenarios as specified in the following:

I. Case 1: two static users (with no mobility) positioned in the centre of the room are facing each other. For this case, we investigate the impact of Rx's orientation on the channel;

II. Case 2: Same as Case 1 above, but while considering mobility for the user holding the Rx;

III. Case 3: combined Cases 1 and 2, i.e., the simulation includes Rx's orientation and mobility of the user holding Rx.

All the key system parameters adopted are given in Table 1.

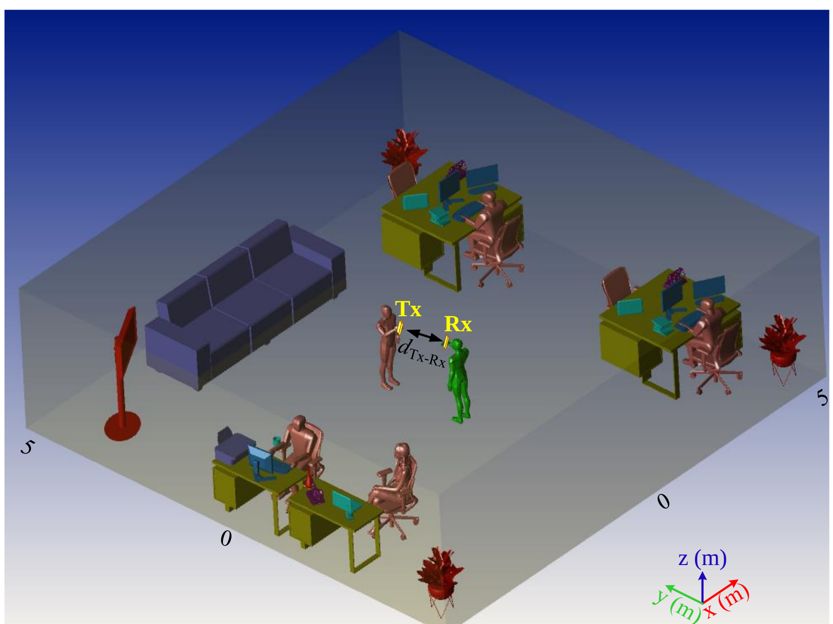

Fig. 1. The three-dimensional indoor environment and proposed scenario showing the locations of the Tx and the Rx.

Table 1. The system parameters

Item	Parameter	Value
Room	Size	10×10×3 m^3
Surface material refractivity in % (RGB)	Chair, sofa (leather)	24, 18.8, 16.3
	Coffee cup (ceramics)	97.1, 96.2, 92.3
	Human clothes (cotton)	67, 58, 45.6
	Plant (leaf)	14, 5.9, 8.2
	Desk, book (pine wood)	70, 51, 33.1
	Laptop, PC, printer, TV, and telephone (black gloss paint)	3.4, 3.2, 3.2
Tx	Dimension	14×7 cm^2
	Power of lighting	1 W
	Number of chip/ LED panel	100
	Power / chip	10 mW
	Height	1.5 m
	Location	(0.5,0,1.5) m
Channel	Time resolution	0.2 ns
	Length $d_{\text{Tx-RX}}$	Case 1: 0.5 m
		Case 2, Case 3: varied (Rayleigh distribution with scale parameter of 0.5)
Rx	Active area of photodiode	1 cm^2
	Responsivity	0.4 A/W
	Field of view	90°
	Height	1.5 m
	Location	Case 1: (-0.5,0,1.5) m
		Case 2, Case 3: varied (see Fig. 3)

2.2 System modelling

We adopt the Rx's orientation about the device coordinate system, see Fig. 2, which is based on the model driven in [21], where the Rx orientation is represented in the spherical coordinates, which follows the polar angle θ with Gaussian distribution with the mean μ_G = 29.7 and standard deviation σ_G = 7.8, and the azimuth angle ω with a uniform distribution ($\omega \sim U[-\pi, \pi)$). Note, a 3D body can be rotated about the three orthogonal axes and in this case θ, which is related to the pitch and roll rotations with the angles of β and γ around the *x*- and *y*- axis, respectively that are associated with the user's wrist movements. The polar and azimuth angles are given, respectively by:

$$\theta = \cos^{-1}(\cos\beta \cos\gamma), \quad (2)$$

$$\omega = \tan^{-1}(\sin\alpha \sin\gamma - \cos\alpha \cos\gamma \sin\beta / \cos\gamma \sin\alpha \sin\beta + \cos\alpha \sin\gamma). \quad (3)$$

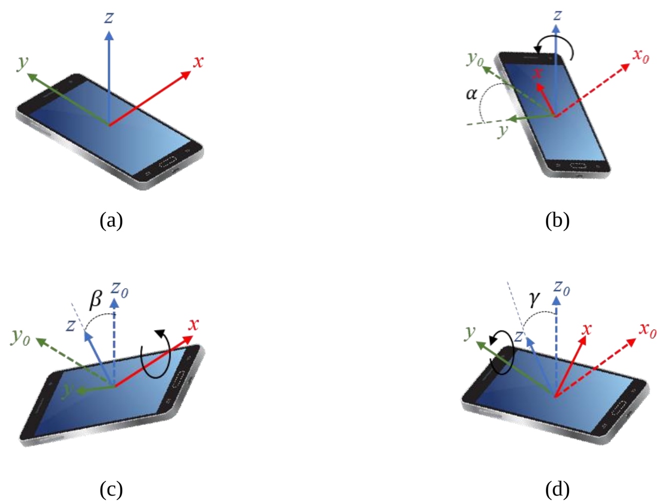

Fig. 2. A model for mobile phone orientation: (a) normal position, (b) around *z* axis with angle of α, (c) around *x* axis with angle of β, and (d) around *y* axis with angle of γ (Ref. [21]).

Using the model given in [21], we have obtained the probability density function (PDF) of the tilt angle values around the *x*- and *y*-axis in the Cartesian coordinates, which unlike the values in [21] can be imported in the simulator, see Fig. 3. We observe the following from Fig. 3: (*i*) the tilt angles around the *x*- and *y*-axis are in the range of -50° to 50°; (*ii*) the symmetrical peaks of 24° and 22° for the *x*- and *y*-axis, respectively; and (*iii*) higher PDF probability by about 0.126 for the *y*-axis at zero tilt angle compared with *x*-axis. The statistics of Rx's orientation might be characterized for the case where the user knows the location of the Tx and, therefore, intentionally orients the Rx towards the Tx. In the simulator, the rotation values for 30 configurations were imported. Rayleigh distribution with the scale parameter $\sigma = 0.5$ was assumed in modelling the user's mobility, see Fig. 4(a) [22]. Further, using Rayleigh distribution, the locations of the Rx in the room with respect to the Tx's location were obtained. Fig. 4(b) shows the map of Rx's locations for 30 positions adopted in the simulation.

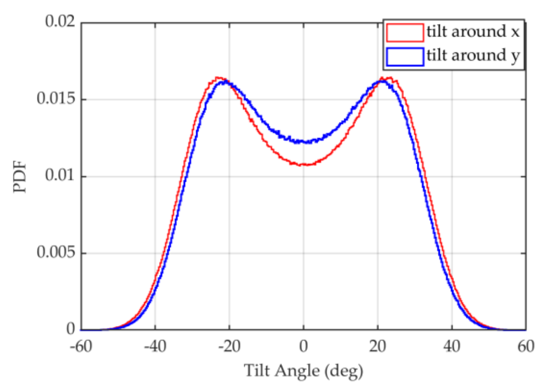

Fig. 3. The PDF of tilt angle values around: (a) *x*, and (b) *y* axis in the cartesian coordinates, obtained from the model in [18].

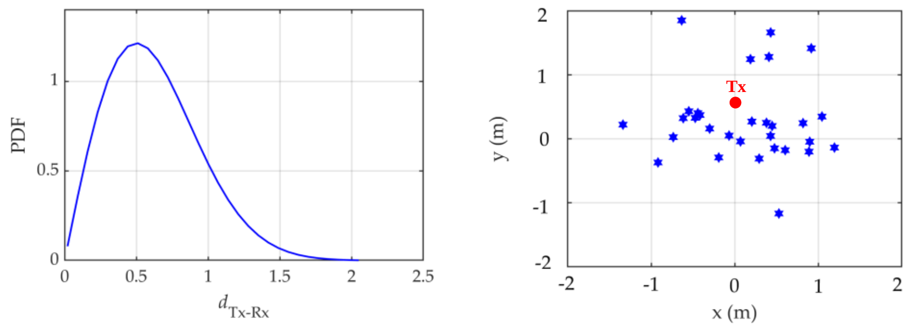

(a) (b)

Fig. 4. Modelling of user mobility: (a) Rayleigh distribution with σ = 0.5 assumed to be comparable with Case 1 where $d_{\text{Tx-Rx}}$ = 0. 5 m, and (b) the map of user movement in the office for 30 positions.

3. Results and Description

The proposed system performance is investigated in terms of the RMS delay spread τ_{RMS} and OPL. The delay spread provides a good estimate of how susceptible the system is to multipath-induced ISI, which leads to reduced R_b. Note, τ_{RMS} is commonly used to define the delay dispersion along the propagation path. The channel mean excess delay τ and the τ_{RMS} are given as [20]:

$$\tau = \frac{\int_0^\infty t \times h(t)dt}{\int_0^\infty h(t)dt}, \tag{4}$$

$$\tau_{RMS} = \sqrt{\frac{\int_0^\infty (t-\tau)^2 \times h(t)dt}{\int_0^\infty h(t)dt}}. \tag{5}$$

The optical signal attenuation caused by reflections and transmission in the free space is quantified by OPL, which is given as [20]:

$$\text{OPL} = -10\log_{10}\left(\int_{-\infty}^{\infty} h(t)dt\right), \tag{6}$$

Figs. 5 and 6 show the PDFs of the channel delay spread τ_{RMS} and OPL for the empty and furnished rooms for Cases 1 and 2. The PDF profiles change with considering user's mobility. A comparison of Cases 1 and 2 in the empty room shows a drop in OPL in Case 2 due to the potential of having lower values of $d_{\text{Tx-Rx}}$. For Case 2, there is a range of probability of OPL from 56 to 64 dB. However, in Case 1, the probability of OPL is restricted to values between 59 to 62 dB. It can be seen that, the range of τ_{RMS} are from 6 to 9 ns, and 5 to 12 ns for Cases 1 and 2, respectively.

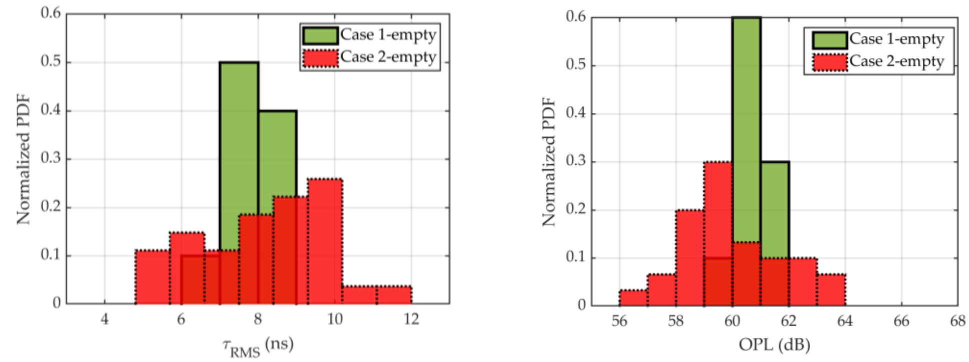

(a) (b)

Fig. 5. The normalized PDF for the Cases 1 and 2 for an empty room: (a) τ_{RMS}, and (b) OPL.

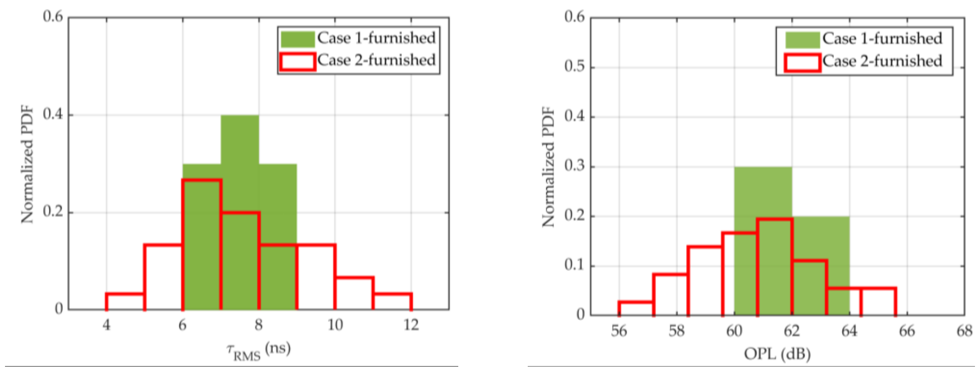

(a) (b)

Fig. 6. The normalized PDF for the Cases 1 and 2 for for a furnished room: (a) τ_{RMS} and (b) OPL.

Fig. 7 shows the comparison of empty and furnished rooms for Case 2. For a furnished room, we can observe a decrease in τ_{RMS} compared with the empty room. However, OPL increases because of increased shadowing and lower values of reflection coefficients for the objects and furniture, compared with the reflection coefficients of the walls. For instance, in Case 2 and for the furnished room, the OPL distribution is risen by 1.5 dB compared with the empty room. For Case 2, in both empty and furnished rooms, τ_{RMS} can reach the maximum value of 12 ns while the delay spread is decreased by 3 ns in the furnished compared with the empty room. It can be seen that the peak of τ_{RMS} are 6.5 and 9.5 ns for the furnished and empty rooms, respectively.

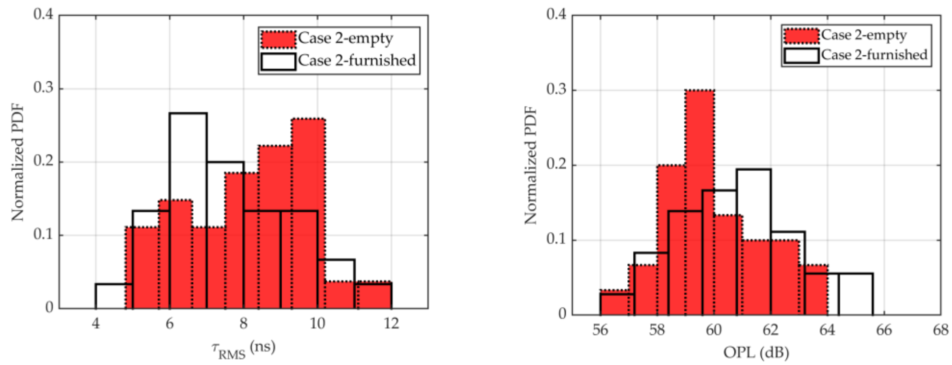

(a) (b)

Fig. 7. The normalized PDF for Cases 2 for the empty and furnished rooms: (a) τ_{RMS}, and (b) OPL.

Fig. 8 depicts the normalized PDF for τ_{RMS} and OPL for Cases 2 and 3 for a furnished room. A numerical fitting method was used to estimate the PDF of τ_{RMS} and OPL for D2D communications where the user mobility and the Rx orientation are considered. Note, Gaussian model provides the best fit to describe the channel characteristics in D2D communications, which is given by:

$$\mathrm{P}(q) = a_1 \exp(-[(q - b_1)/c_1]^2), \tag{7}$$

where q is τ_{RMS} or OPL, a_1, b_1, and c_1 are the parameters estimated by the curve fitting, which are further summarized in Tables 2 and 3 for τ_{RMS} or OPL, respectively. The root mean square error (RMSE) value of the statistical model is less than a standard error limit of 0.05 to assess the accuracy of the model. i.e., RMSE $=\sqrt{\sum(P_s - P_m)^2/n}$, where P_s and P_m are the values obtained from simulation and statistical model, respectively and n is the number of modelled samples. We can see, OPL increases for Case 3, e.g., the mean value of Gaussian model is 62 dB; however, it drops to 60 dB for Case 2. In addition, for Case 3 the delay spread is also increasing, e.g., the mean of Gaussian distribution is 6.99 ns, however, it drops to 6.78 ns for Case 2. For Case 3, the increase in τ_{RMS} and OPL for Gaussian model compared with Case 2 is due to considering the Rx's orientation. However, the results show that even for the worst-case scenario i.e., including the Rx's mobility and its orientation, the achieved PDF of τ_{RMS} demonstrates the feasibility of OVLC for D2D communications.

Table 2. Numerical modelling parameters for τ_{RMS}.

Scenario	Parameter
Case 2-furnished	
a_1	0.22
b_1	6.78
c_1	2.55
Case 3-furnished	
a_1	0.24
b_1	6.99
c_1	2.41

Table 3. Numerical modelling parameters for OPL.

Scenario	Parameter
Case 2-furnished	
a_1	0.17
b_1	60.13
c_1	3.44
Case 3-furnished	
a_1	0.17
b_1	61.94
c_1	3.53

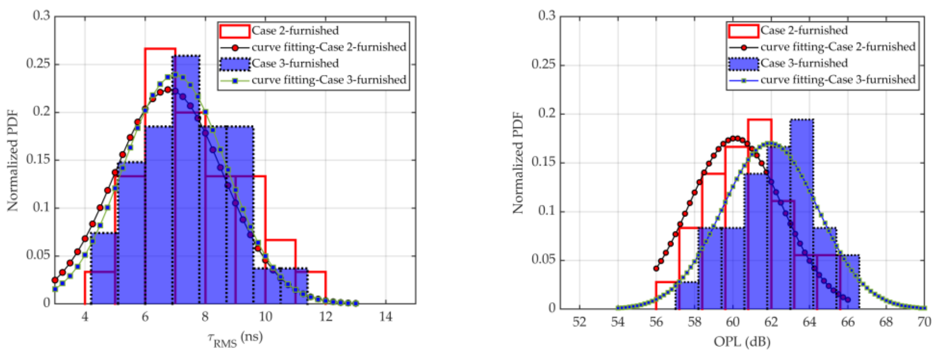

(a) (b)

Fig. 8. The normalized PDF for the cases 2 and 3 for : (a) τ_{RMS}, and (b) OPL.

Table 4 shows the comparison of the highest PDF values for τ_{RMS} and OPL for three cases.

Table 4. A comparison of the maximum PDF values for τ_{RMS} and OPL for all three cases.

Scenario	Maximum PDF	
	OPL (dB)	τ_{RMS} (ns)
Case 1-empty	60.5	7.5
Case 1-furnished	61	7.5
Case 2-empty	59	9.5
Case 2-furnished	60	6.78
Case 3-furnished	62	6.99

Using Gaussian distribution model for OPL, see Fig. 8, the normalized PDF for the channel capacity was obtained for Cases 2 and 3 for a furnished room as shown in Fig. 9. The channel capacity has the mean values of 15 and 7 Mb/s for Cases 2 and 3, respectively. However, the PDF plot shows that the channel capacity reaches up to 50 Mb/s with the PDF values of 0.11 and 0.41 for Cases 2 and 3, respectively.

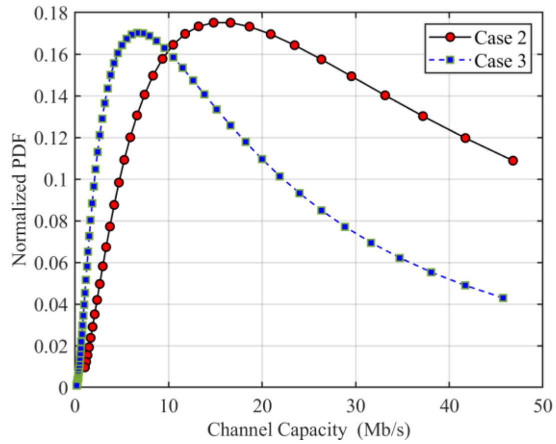

Fig. 9. The normalized PDF for the cases 2 and 3 for the channel capacity at R_b of 4 Mb/s and and optical power of 5 W.

4. Conclusion

An OVLC-based D2D communications scheme was considered in this paper, with the aim of investigating the impact of Rx random orientations on the channel characteristics. In addition, to demonstrate the feasibility of D2D communications in more realistic application scenarios, the user's mobility was investigated by means of simulation. We showed that, considering random Rx's orientation, the maximum values of OPL for the empty and furnished rooms were about 62 and 64 dB, respectively. However, there was a drop in τ_{RMS} for the furnished room compared with the empty room. When including user mobility, the peak τ_{RMS} in the empty room was about 9.5 ns, which dropped to 6.5 ns for the case of furnished room. Additionally, to evaluate the accuracy of the model we approximated the PDFs of τ_{RMS} and OPL by Gaussian distributions, where the RMSE value was less than a standard error limit of 0.05. We showed that in the case of Rx's orientation and including user mobility, OPL can be found as a Gaussian model with the mean value of 62 dB which expresses the feasibility of OVLC-based D2D communications in indoor environments.

Acknowledgement

This work is supported by the European Union's Horizon 2020 research and innovation programme under the Marie Sklodowska-Curie grant agreement no 764461 (VISION), and COST Action CA19111 NEWFOCUS. The work of Zahra Nazari Chaleshtori was supported by CTU project SGS20/166/OHK3/3T/13.

References

1. Z. Ghassemlooy, L. N. Alves, S. Zvanovec, and M. A. Khalighi, Visible Light Communications: Theory and Applications. CRC-Press, 2017.
2. Z. Ghassemlooy, W. Popoola, and S. Rajbhandari, Optical wireless communications: system and channel modelling with Matlab®. 2nd Edition. CRC press, NY, 2019.
3. J. Kalinowski, Organic Light-Emitting Diodes: Principles, Characteristics & Processes. CRC press, 2018.
4. P. A. Haigh, Z. Ghassemlooy, S. Zvánovec, and M. Komanec, "VLC with Organic Photonic Components," in Visible Light Communications: Theory and Applications: CRC Press, pp. 521-548, 2017.
5. S. Long, M. A. Khalighi, M. Wolf, S. Bourennane, and Z. Ghassemlooy, "Investigating channel frequency selectivity in indoor visible light communication systems." Iet Optoelectronics, 10(3), 2016, pp. 80-88.
6. H. Chun, C.-J. Chiang, and D. C. O'Brien, "Visible light communication using OLEDs: Illumination and channel modeling," in 2012 International Workshop on Optical Wireless Communications (IWOW), 2012: IEEE, pp. 1-3.

7. K. Lee, H. Park, and J. R. Barry, "Indoor channel characteristics for visible light communications," IEEE Communications Letters, vol. 15, no. 2, pp. 217-219, 2011.
8. S. P. Rodríguez, R. P. Jiménez, B. R. Mendoza, F. J. L. Hernández, and A. J. A. Alfonso, "Simulation of impulse response for indoor visible light communications using 3D CAD models," EURASIP Journal on Wireless Communications and Networking, vol. 2013, no. 1, p. 7, 2013.
9. Zemax OpticStudio 18.9, [Online]. Available: https://www.zemax.com/products/opticstudio
10. F. Miramirkhani and M. Uysal, "Channel modeling and characterization for visible light communications," IEEE Photonics Journal, vol. 7, no. 6, pp. 1-16, 2015.
11. M. Uysal, F. Miramirkhani, O. Narmanlioglu, T. Baykas, and E. Panayirci, "IEEE 802.15. 7r1 reference channel models for visible light communications," IEEE Communications Magazine, vol. 55, no. 1, pp. 212-217, 2017.
12. X. Nan, P. Wang, L. Guo, L. Huang, and Z. Liu, "A novel VLC channel model based on beam steering considering the impact of obstacle," IEEE Communications Letters, vol. 23, no. 6, pp. 1003-1007, 2019.
13. H. Chen and Z. Xu, "OLED panel radiation pattern and its impact on VLC channel characteristics," IEEE Photonics Journal, vol. 10, no. 2, pp. 1-10, 2017.
14. Z. Nazari Chaleshtori, Z. Ghassemlooy, H.B. Eldeeb, M. Uysal, and S. Zvanovec, "Utilization of an OLED-Based VLC System in Office, Corridor, and Semi-Open Corridor Environments", *Sensors*, vol. 20, no. 23, pp.6869, 2020.
15. S. H. Younus, A. A. Al-Hameed, J. M. Elmirghani, “Multi-user high data rate indoor VLC systems.” *IETE Journal of Research*, pp.1-14, 2020.
16. J. Wei, C. Gong, N. Huang, and Z. Xu, “Channel Modeling and Signal Processing for Array-based Visible Light Communication System in Misalignment.” *arXiv preprint arXiv:2101.03548*. 2021.
17. H. B. Eldeeb, S. M. Mana, V. Jungnickel, P. Hellwig, J. Hilt, M. and Uysal, “Distributed MIMO for Li-Fi: Channel Measurements, Ray Tracing and Throughput Analysis.” *IEEE Photonics Technology Letters*, 2021.
18. I. Jun, S. J. Han, H. S. Shin, J. Kim, E. K. Kim, S. C. Yoon, and K. Y. Seo, “Comparison of ophthalmic toxicity of light-emitting diode and organic light-emitting diode light sources.” *Scientific reports*, vol. 10(1), pp.1-10, 2020.
19. Z. Nazari Chaleshtori, A. Burton, S. Zvanovec, Z. Ghassemlooy, and P. Chvojka, “Comprehensive optical and electrical characterization and evaluation of organic light-emitting diodes for visible light Communication.” *Optical Engineering*, vol. 59(4), pp.046106, 2020.
20. Z. Nazari Chaleshtori, S. Zvanovec, Z. Ghassemlooy, H. B. Eldeeb, and M. Uysal, “Coverage of a shopping mall with flexible OLED-based visible light communications.” *Optics express*, vol. 28(7), pp.10015-10026, 2020.
21. M.D. Soltani, A. A. Purwita, Z. Zeng, H. Haas, and M. Safari, "Modeling the random orientation of mobile devices: Measurement, analysis and LiFi use case," IEEE Transactions on Communications, vol. 67, no. 3, pp.2157-2172, 2018.
22. Y.S. Eroğlu, Y. Yapıcı, and I. Güvenç, "Impact of random receiver orientation on visible light communications channel." IEEE Transactions on Communications, 67(2), pp.1313-1325, 2018.